

FBA²D: Frequency-based Black-box Attack for AI-generated Image Detection

Xiaojing Chen, Dan Li, Lijun Peng, Jun Yan✉, Zhiqing Guo,
Junyang Chen, Xiao Lan, Zhongjie Ba, Yunfeng Diao✉

Abstract

*The prosperous development of Artificial Intelligence-Generated Content (AIGC) has brought people’s anxiety about the spread of false information on social media. Designing detectors for filtering is an effective defense method, but most detectors will be compromised by adversarial samples. Currently, most studies exposing AIGC security issues assume information on model structure and data distribution. In real applications, attackers query and interfere with models that provide services in the form of application programming interfaces (APIs), which constitutes the black-box decision-based attack paradigm. However, to the best of our knowledge, decision-based attacks on AIGC detectors remain unexplored. In this study, we propose **FBA²D**: a frequency-based black-box attack method for AIGC detection to fill the research gap. Motivated by frequency-domain discrepancies between generated and real images, we develop a decision-based attack that leverages the Discrete Cosine Transform (DCT) for fine-grained spectral partitioning and selects frequency bands as query subspaces, improving both query efficiency and image quality. Moreover, attacks on AIGC detectors should mitigate initialization failures, preserve image quality, and operate under strict query budgets. To address these issues, we adopt an “adversarial example soup” method, averaging candidates from successive surrogate iterations and using the result as the initialization to accelerate the query-based attack. The empirical study on the Synthetic LSUN dataset and Gen-Image dataset demonstrate the effectiveness of our prosed method. This study shows the urgency of addressing practical AIGC security problems.*

1. Introduction

The explosion of AIGC technology has greatly enriched people’s entertainment. This technology relies on generative models, such as Generative Adversarial Networks (GANs) [17] and diffusion models [20], which can generate realistic content. However, synthetic content can be exploited for illegal purposes, such as the dissemination of false information, raising public concern over the potential

misuse of these technologies.

Ensuring the integrity of digital media requires reliable detection of AIGC, a challenge that has attracted significant interest in both academia and industry. State-of-the-art detectors [37, 44] predominantly leverage deep neural networks to discriminate between authentic and generated examples, demonstrating strong performance across diverse datasets and generative models. Compared with deepfake detection [38], which is a vertical, person-centric forensics task emphasizing temporal cues and physiological consistency, AIGC detection focuses more on cross-modal forensics, frequency-domain evidence, and semantic-consistency checks.

These DNN-based detectors remain vulnerable to adversarial perturbations—imperceptible, carefully crafted modifications that can mislead the classifier [18]. Existing methods have presented the adversarial vulnerability of AIGC detectors [10, 30, 34], but these methods require access to the detector’s network architecture or dataset. However, in practical applications, attackers cannot obtain this prior knowledge and will only receive a detection output. In this black-box threat model, the adversary can only query the hard label output of the classifier, having no access to its architecture, weights, confidence scores, or gradients. This attack is known as a decision-based attack. To the best of our knowledge, the research on decision-based attacks against AIGC detectors is insufficient. Unlike the multi-classification task of image classification, AIGC detection is usually defined as a binary classification problem to distinguish generated content from real content. Existing decision-based attacks usually use random noise as attack initialization, which is easy to succeed in image classification tasks. Nevertheless, the real-fake binary classification in AIGC detection is different from the common and standard cat and dog binary classification in that the binary classification of AIGC detection is asymmetric [41], that is, the characteristics of the generated content only exist in a small decision area. It is difficult to initialize in this small decision area using random noise as attack initialization. The adversary can overcome this difficulty by launching a direct targeted attack. But it suffers from degraded image quality and an excessive number of queries. In practical application

scenarios, the number of queries is usually limited. Therefore, it is significant to explore the decision-based black-box attack method against AIGC detectors. Furthermore, previous studies have shown that the distribution of generated images and real images in the frequency domain is different [2, 16]. Compared with real images, the information of generated images is more concentrated in the low-frequency area, and the information in the high-frequency area is sparse.

To fill such a research gap, we propose an efficient frequency-based black-box adversarial attack method to expose the vulnerability of the AIGC detectors. Figure 1 illustrates our proposed framework. Specifically, the AI-generated images usually exhibit unnatural energy distribution patterns in high frequency components [12] with the specific fingerprints [29]. Thus, we select different strategies for real and generated images due to their frequency domain characteristics. For real images, we employ a mixed high- and low-frequency band as the query subspace. For generated images, we restrict the query subspace to the low-frequency band, which can improve query efficiency and image quality. To improve the efficiency of the query-based attack, we use the “example soup” method [43] to obtain the average adversarial examples of the surrogate model at different iterations and query whether this average adversarial example is adversarial when attacking the target model. If the sample is adversarial, we use the averaged adversarial example as the initial perturbation of the decision-based attack. If the average example is not adversarial, we instead use the targeted attack method and employ data from another category as the initial perturbation to ensure the success of initialization. In the empirical study, our method achieves state-of-the-art attack performance and query efficiency on the Synthetic LSUN dataset [37] and the Gen-Image benchmark [47], further providing some inspiration for the security performance of AIGC detectors in real scenarios. Unlike DeepFake detectors, which primarily rely on facial symmetry, temporal coherence, or physiological consistency [38], AIGC detectors are often sensitive to distinct high-frequency noise patterns, color statistics, and texture cues arising from generative models. Our proposed method is the first decision-based black-box attack method specifically tailored to this new AIGC detection task, featuring a novel frequency-aware perturbation scheme and optimization strategy. Our main contributions are summarized as follows.

- To the best of our knowledge, this study proposes the first decision-based attack method for AIGC models, which adapts to the security assessment requirements of real detection scenarios.
- Our experimental results show that real images contain low-frequency and high-frequency components, and generated images mainly contain low-frequency components.

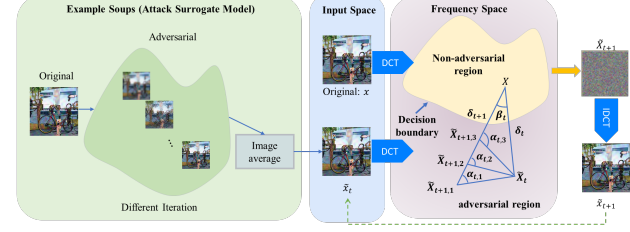


Figure 1. Our proposed FBA²D framework.

- Building on our empirical insights in the frequency domain, we further refine our decision-boundary attacks. For real images, we define the query subspace as the combined low- and high-frequency components. In contrast, for generated images, our black-box attack restricts queries to the low-frequency subspace, improving both query efficiency and the quality of the crafted adversarial examples.

2. Related Work

2.1. Decision-based Attacks

In the scenarios of black-box adversarial attacks, the assailant would not require access to the internal structure of the target model to carry out attacks, including transfer-based [13], score-based [19, 25], and decision-based [1, 4, 7, 31] attacks. These studies are closely related to the real-world security issues.

Brendel et al. [1] proposed the first decision-based attack method, known as Boundary Attack, in which the attacker iteratively adjusts examples to maintain adversarial properties while moving toward the decision boundary. Subsequent works such as GeoDA [31] and Triangle Attack [39] provide the geometric information to explore the decision boundary, thus improving the efficiency of the attack. The OPT method [7] leverages the zeroth-order optimization method and demonstrates strong performance in reducing query complexity. The Sign-OPT method efficiently estimates the gradient direction, accelerating the process of black-box attacks [8]. The SignFlip method [6] introduces noise projection and random sign flipping, significantly improving decision-based attacks. The HSJA method [4] uses the geometric properties of high-dimensional spaces and performs well in complex models. The RayS method [3] reformulates the continuous problem of finding the nearest decision boundary into a discrete one, eliminating the need for zeroth-order gradient estimation. While these methods are primarily used for image classification tasks, their effectiveness in AIGC security has not been fully explored.

2.2. Adversarial Robustness of AIGC Detectors

AIGC detection is a security-sensitive task, which is vulnerable to adversarial examples [10, 30, 34]. Early stud-

ies have revealed that GAN-generated images have artifact features in frequency domains [15, 16]. To this end, a variety of high-accuracy frequency domain detection methods [2, 16] have been proposed to resolve this problem. Dong et al. [11] demonstrated the reliability limitations of frequency artifact-based detection methods. Research on adversarial attacks against detectors has evolved in multiple dimensions. Diao et al. [10] conducted the first systematic evaluation of AIGC detector vulnerabilities in both white-box and transfer-based black-box scenarios. Saberi et al. [34] established robustness benchmarks for digital watermarking and classifier-based detection methods. In terms of attack techniques, Lee et al. [24] proposed the Spectrum Translation for Refinement of Image Generation (STIG) framework, which enhances the stealthiness of adversarial examples through spectral transformation optimization of generated images. Zhou et al. [45] proposed a StealthDiffusion method, which effectively evades state-of-the-art forensic detectors. Our study launches a decision-based attack against the AIGC detector to provide insight into the security of AI content in real-world applications.

3. Method

In this study, we propose **FBA²D**: a decision-based attack method for AI-generated image detection. Fig.1 illustrates our proposed method. This method is inspired by the milestone work [39]. We scale the Triangle Attack paradigm to the AIGC detection scenario with a new frequency-domain signal adjustment mechanism. The clean data x would be attacked as adversarial examples $\tilde{x}_t, \tilde{x}_{t+1}$ in the current and next queries. In the frequency space, we apply the DCT to adjust the signals, where the variables $X_t, \tilde{X}_{t+1,1}, \tilde{X}_{t+1,2}, \tilde{X}_{t+1,3}$ denote the adversarial data of different queries t in the frequency domain, and the variables δ_t, δ_{t+1} represent the perturbations. The variables $\alpha_{t,1}, \alpha_{t,2}, \alpha_{t,3}, \beta_t$ represent the search angles in the decision boundary. To improve the efficiency of the attack, we introduce the concept of “Adversarial Example Soups” (AES). The Projected Gradient Descent (PGD) method is applied to configure a successful initialization with iterations I_1, \dots, I_n to transform n original natural samples into adversarial examples for the average operation. The attack on the surrogate model further boosts the attack effectiveness and efficiency of the decision-based attack on the AIGC detector.

3.1. Preliminaries

We define an AI-generated content detector $f : \mathbb{R}^d \rightarrow \mathbb{R}^k$ as the detection model. Because AIGC detection is a binary classification task, its label y is real or fake. The formulation is $y \in \mathbb{R}^2 = \{0, 1\}$. Given an original image x , we define $f(x)$ as the detector function and $c(x) = \arg \max f(x)$ as the predicted label. In the decision-based attack, the ad-

versary has no access to the network architecture, weights, gradients, or predicted probabilities of the model $f(x)$, only the predicted labels of the model $c(x)$. Therefore, the optimization objective of the decision-based attack is as follows:

$$\min_{\delta} \|\delta\|_p \quad \text{s.t.} \quad c(x + \delta) \neq c(x), \quad (1)$$

where the adversary keeps querying the model and optimizing adversarial perturbations δ until $\|\delta\|_p \leq \epsilon$, and ϵ is the allowed maximum perturbation.

3.2. Frequency Perspective on Adversarial Robustness in AIGC Detection

Recent advances in AIGC detection have systematically characterized the pronounced frequency domain disparities between real and AI-generated [2, 16], with state-of-the-art detectors achieving discrimination by capitalizing on these spectral signatures [37]. Most of these studies find that, compared to generated images, real images contain richer high-frequency components. Motivated by these findings, we propose a decision-based attack method to fully exploit the frequency-dependent characteristics of generated versus real images across different model architectures.

The baseline method we employ unifies geometric optimization paradigms with signal frequency-domain analysis [39] to achieve multi-band perturbation synthesis through spatial iterations and frequency-domain transformations. This method treats the input space as a signal field, deconstructing adversarial perturbations using spectral tools. The baseline is a query-efficient decision-based adversarial attack method that has good results on classification tasks. However, previous studies have shown that the binary classification problem of AIGC detection is not the same as the traditional cat-dog binary classification problem. The binary classification of AIGC detection is asymmetric [41], that is, the probability of being classified into one category may be higher than the probability of being classified into the other category. The decision-based attack mechanism [39] that works in image classification cannot be directly applied to AIGC detection tasks. Specifically, the initialization of the decision-based attack fails, resulting in an attack success rate close to 0%. It shows that random initialization is unsuccessful and cannot guarantee adversarial behavior. Therefore, we use a targeted attack to ensure a successful initialization.

In the previous classification task, the attack is built on the postulation that the image gradient estimation was concentrated in the low-frequency domain. Thus, the adversary would use the low-frequency frequency domain (the upper 10% frequency components) as the query subspace to improve the query efficiency. When facing the AIGC detection task, the frequency domain difference between the generated image and the real image will lead to a difference in the attack paradigm. Consequently, we partition the

Algorithm 1 Decision-based Attack for AI-generated Image Detection

Input: Detection model f ; Original data x with ground-truth label y ; target adversarial example x_t from a category different from that of the original data x ; Maximum number of queries Q ; Maximum number of iteration N for each sampled subspace; Dimension of the directional line d ; Lower bound $\underline{\beta}$ for angle β .
Parameter: The learned angle α , and the search angle β .
Output: An adversarial example \tilde{x} .

```

1: Initialize an adversarial example  $\tilde{x}_0 = x_t$ ;
2:  $\tilde{X}_0 = \text{DCT}(\tilde{x}_0)$ ,  $X = \text{DCT}(x)$ ,  $q = 0$ ,  $t = 0$ ,  $\alpha_0 = \pi/2$ ;
3: while  $q < Q$  do
4:   Sample 2-D subspace  $\mathcal{S}_t$  in the frequency-domain;
5:    $\beta_{t,0} = \max(\pi - 2\alpha_t, \underline{\beta})$ ;
6:   if  $c(\mathcal{T}(X, \tilde{X}_t, \alpha_{t,0}, \beta_{t,0}, \mathcal{S}_t)) = c(X)$  then
7:      $q = q + 1$ ;
8:     Update  $\alpha_{t,0}$  based on Eq. (5);
9:     if  $c(\mathcal{T}(X, \tilde{X}_t, \alpha_{t,0}, -\beta_{t,0}, \mathcal{S}_t)) = c(X)$  then
10:     $q = q + 1$ ;
11:    Update  $\alpha_{t,0}$  based on Eq. (5);
12:    Go to the next loop iteration;
13:   end if
14:   end if
15:    $\beta_{t,0} = \min(\pi/2, \pi - \alpha_t)$ ;
16:   for  $i = 0 \rightarrow N$  do
17:      $\beta_{t,i+1} = (\bar{\beta}_{t,i} + \beta_{t,i})/2$ ;
18:     if  $c(\mathcal{T}(X, \tilde{X}_t, \alpha_{t,i}, \beta_{t+1,i}, \mathcal{S}_t)) = c(X)$  then
19:        $q = q + 1$ ;
20:       Update  $\alpha_{t,0}$  based on Eq. (5);
21:       if  $c(\mathcal{T}(X, \tilde{X}_t, \alpha_{t,i}, -\beta_{t+1,i}, \mathcal{S}_t)) = c(X)$  then
22:          $\bar{\beta}_{t,i+1} = \beta_{t,i+1}$ ,  $\beta_{t,i+1} = \beta_{t,i}$ ;
23:       end if
24:     end if
25:      $q = q + 1$ ;
26:     Update  $\alpha_{t,i+1}$  based on Eq. (5);
27:   end for
28:    $\tilde{X}_{t+1} = \mathcal{T}(X, \tilde{X}_t, \alpha_{t,i+1}, \beta_{t,i+1}, \mathcal{S}_t)$ ,  $t = t + 1$ ;
29: end while
30: return  $\tilde{x}_t = \text{IDCT}(\tilde{X}_t)$ .

```

frequency spectrum into distinct bands and evaluate, within each subspace, the quality and attack success rate of adversarial examples crafted from real versus generated images.

To ensure successful initialization, we employ a targeted attack strategy by selecting the target example x_t from a category different from that of the input image x , that is $c(x_t) \neq c(x)$. This target example will serve as our initial adversarial example $\tilde{x}_0 = x_t$. Then, we apply the DCT to

both the input image and the initial adversarial example:

$$X = \text{DCT}(x), \quad \tilde{X}_0 = \text{DCT}(\tilde{x}_0), \quad (2)$$

where X is the frequency-domain representation of x obtained through the DCT module. To explore the distribution of gradient estimation between real and generated images, we utilize different frequency-domain segments as query subspaces for investigating the decision boundary based on the geometric information.

3.2.1. Subspace Sampling

We randomly sample a d -dimensional directional line v_{rand} in the frequency domain, which together with the current adversarial example \tilde{X}_t direction determines a 2-D subspace $\mathcal{S}_t = \text{span}(v_{\text{rand}}, \tilde{X}_t - X)$, where span is the vector space formed by all possible linear combinations of a given set of vectors. The core methodology is to employ triangular geometric properties for adversarial perturbation optimization. At each iteration, the input example X , current adversarial example \tilde{X}_t and next adversarial example \tilde{X}_{t+1} can naturally form a triangle in a subspace. According to the law of sines (suppose a , b and c are the side lengths of a triangle, and α , β and γ are the opposite angles, we have $\frac{a}{\sin \alpha} = \frac{b}{\sin \beta} = \frac{c}{\sin \gamma}$), we have the following relationship:

$$\frac{\delta_t}{\sin \alpha_t} = \frac{\delta_{t+1}}{\sin(\pi - (\alpha_t + \beta_t))}, \quad (3)$$

where $\delta_t = \|\tilde{X}_t - X\|_p$ is the current perturbation magnitude, α_t is the learned angle, β_t is the search angle. To greedily decrease the perturbation (i.e., $\delta_{t+1} < \delta_t$), the following condition should satisfy the formulation as follows:

$$\beta_t + 2\alpha_t > \pi. \quad (4)$$

3.2.2. Candidate Triangle Search

In the current subspace, we search for adversarial examples based on angle constraints. We first initialize the search angle $\beta_{t,0} = \max(\pi - 2\alpha_t, \underline{\beta})$, where $\underline{\beta} = \pi/16$. If neither $\mathcal{T}(X, \tilde{X}_t, \alpha_t, \beta_{t,0}, \mathcal{S}_t)$ nor $\mathcal{T}(X, \tilde{X}_t, \alpha_t, -\beta_{t,0}, \mathcal{S}_t)$ is adversarial, we give up this subspace because it cannot bring any benefit, where $\mathcal{T}(\cdot)$ is the geometric transformation function that generates the next adversarial example based on triangle constraints in subspace \mathcal{S}_t . Otherwise, we use binary search to find the optimal angle β^* in the interval $[\max(\pi - 2\alpha_t, \underline{\beta}), \min(\pi - \alpha_t, \pi/2)]$. Finally, we calculate the position of the new adversarial example $\tilde{X}_{t+1} = \mathcal{T}(X, \tilde{X}_t, \alpha_t, \beta^*, \mathcal{S}_t)$.

3.2.3. Adaptive Angle Adjustment

Intuitively, the angle α balances the magnitude of perturbation and the difficulty to find an adversarial example, we

dynamically adjust the learned angle α based on search results:

$$\alpha_{t,i+1} = \begin{cases} \min(\alpha_{t,i} + \gamma, \frac{\pi}{2} + \tau) & \text{if } c(\tilde{X}_{t,i+1}) \neq c(X) \\ \max(\alpha_{t,i} - \lambda\gamma, \frac{\pi}{2} - \tau) & \text{otherwise} \end{cases} \quad (5)$$

, where $\tilde{X}_{t,i+1} = \mathcal{T}(X, \tilde{X}_t, \alpha_{t,i}, \beta_t^*, \mathcal{S}_t)$ is the adversarial example generated by $\alpha_{t,i}$, γ is the change rate, λ is a constant, and τ restricts the upper and lower bounds of α . We adopt $\lambda < 1$ to prevent decreasing the angle too fast considering much more failures than successes during the perturbation optimization. Note that the larger angle α makes it harder to find an adversarial example. However, a too small angle α results in a much lower bound for β , which also makes $\mathcal{T}(X, \tilde{X}_t, \alpha_t, \beta^*, \mathcal{S}_t)$ far away from the current adversarial example \tilde{X}_t , decreasing the probability to find an adversarial example. Thus, we add the bounds for α to restrict it in an appropriate range. All geometric operations are performed in DCT frequency domain, then mapped back to image space via Inverse Discrete Cosine Transform (IDCT):

$$\tilde{x} = \text{IDCT}(\tilde{X}), \quad (6)$$

where \tilde{x} is the adversarial example that is finally transformed back to the spatial domain.

Our research is inspired by the different frequency domain characteristics of real images and generated images. After conducting hypothesis-informed experiments on different frequency domain subspaces, we find that the gradient estimation of real images is more concentrated in the low-frequency and high-frequency parts, while the gradient estimation of generated images is more concentrated in the low-frequency part. In view of this, we use the high-low mixed frequency-domain as the subspace for real images and the low frequency-domain subspace for generated images. We iteratively search for candidate triangles to find adversarial samples and update the angle α accordingly.

3.3. Efficient Initialization Based on “Adversarial Example Soup”

To further improve query efficiency, we introduce the paradigm of adversarial example soup [43] for our efficient initialization. In AIGC-related security research, transfer-based attacks can generate adversarial samples via public surrogate models and directly launch black-box attacks against target detectors [10]. But when the surrogate model and the target model differ significantly in structure, the attack effectiveness may be compromised. Our approach fundamentally differs from conventional transfer-based attacks by repurposing their attack outputs exclusively as initialization inputs for our framework. Initializing decision-based attacks with the results of transfer-based attacks can ensure both attack effectiveness and query efficiency.

We use the variable θ to represent the parameters of the surrogate model F . For optimization, $L(\theta, x, y)$ denotes the loss function of the surrogate model. The formulation of the generating adversarial examples x^{adv} can be written as follows:

$$\arg \max_{x^{\text{adv}}} L(\theta, x^{\text{adv}}, y), \quad \text{s.t. } \|x^{\text{adv}} - x\|_p \leq \varepsilon, \quad (7)$$

where x is the original image, y is the ground label, ε is the allowed maximum perturbation.

During the generation of adversarial examples, we take the Momentum Iterative Gradient (MIG) method as an example [28]. At each iteration, MIG updates the adversarial example by accumulating momentum (exponentially weighted average of past gradients):

$$g_{t+1} = \mu \cdot g_t + \frac{\nabla_x L(\theta, x_t^{\text{adv}}, y)}{\|\nabla_x L(\theta, x_t^{\text{adv}}, y)\|_1}, \quad (8)$$

$$x_{t+1}^{\text{adv}} = \text{Clip}_{x, \varepsilon}(x_t^{\text{adv}} + \eta \cdot \text{sign}(g_{t+1})), \quad (9)$$

where g_t denotes the momentum gradient at the t -th iteration, μ is the momentum decay factor, η is the step size, x_t^{adv} is the adversarial example at the t -th iteration. Then, our method preserves n adversarial examples from both optimal and suboptimal iterations, generating the final adversarial example $x_{\text{avg}}^{\text{adv}}$ through ensemble averaging. The formulation is $x_{\text{avg}}^{\text{adv}} = \sum_{i=1}^n w_i x_i^{\text{adv}}$, where it satisfies $w_i = 1/n$. In the final stage, the generated $x_{\text{avg}}^{\text{adv}}$ is given to our detection model for evaluation. When the sample soup is adversarial, that is $c(x_{\text{avg}}^{\text{adv}}) \neq c(x)$, it serves as the initial point for the decision-based attack. In cases of failure, the algorithm defaults back to the standard targeted attack procedure. Our proposed FBA²D method is presented as Algorithm 1. Using triangular geometry properties and frequency domain optimization, it exposes vulnerabilities in AIGC detectors. Concurrently, we accelerate attacks using adversarial example soups or transfer-based attacks.

4. Experiment

4.1. Experiment Settings

4.1.1. Datasets

We choose Synthetic LSUN dataset [37] and GenImage dataset [47] as our evaluation benchmarks. Details of the datasets are provided in the appendix.

4.1.2. Evaluated Models

We evaluate our proposed method on the following prominent AIGC detector architectures: CNNSpot [37], DenseNet [22], EfficientNet [35], MobileNet [21], Vision Transformer (ViT) [14], Swin Transformer [27], PatchCraft [44], AIDE [40], and Effort [42].

4.1.3. Compared Methods

We employ the HopSkipJumpAttack (HSJA) method [5], which leverages high-dimensional geometric properties. Two frequency-based attack methods are Geometric-based Attack [32] and TA [39] methods. OPT is a milestone generic and optimization-based hard-label black box attack method [7]. Sign-OPT [8] resolves the query efficiency bottleneck in hard-label black-box attacks through its core principle of gradient sign estimation coupled with directional aggregation. We also include the Approximation Decision Boundary Attack (ADBA) method [36], which uses the distribution’s median value as the approximation to differentiate the perturbation directions with high query efficiency. To ensure a fair comparison, all attacks are limited to 500 queries, and we report the attack success rate, the average number of queries, and the average ℓ_2 distance at the Root Mean Squared Error (RMSE) threshold of 0.1, 0.05, and 0.01. The implementation details of our experiment are provided in the appendix.

4.2. Experimental Results

The experiments we would conduct are primarily designed to address several questions concerning decision-based attacks on AIGC detectors. Adversarial attacks against AIGC detectors exhibit markedly different characteristics from those observed in conventional image classification. AIGC detectors must grapple with more complex multimodal data and generator-specific attributes, whereas image classifiers primarily focus on pixel-level perturbations and gradient estimation. This divergence stems from two key factors. First, there exists an inherent asymmetry in the detection task. The real world contains a vast number of real images, whereas synthetic images are relatively scarce. Second, image classifiers depend on semantic understanding to recognize objects. Although AI-generated images share similar semantic features with real images, they evoke different perceptual experiences. Prior work has attributed this discrepancy to the relative scarcity of high-frequency components in generated images [2, 16]. Building on these insights, our experiments will systematically investigate the following questions.

- **Q:** Considering the fundamental differences between AIGC detection and conventional classification, and the divergent frequency domain signatures of generated versus real images, how can decision-based attacks with frequency domain transformation be more effectively tailored to the AIGC detection task? **A:** We conduct experiments across multiple frequency bands to analyze how the signal information of generated and real images is distributed throughout the frequency spectrum.
- **Q:** How do we evaluate the effectiveness of the method? **A:** We perform a comprehensive, multi-dimensional assessment, considering the attack success rate, the number

of queries, and the visual quality of the adversarial examples.

- **Q:** What is the purpose of the adversarial example soup with the initialization of transfer-based attack? **A:** We introduce the concepts of adversarial example soups and transfer-based attacks to optimize the initialization of decision-based attacks, thereby improving query efficiency.

4.2.1. Main Results

Table 1 and Table 2 show the attack results of the mainstream decision-based attack methods on the LSUN [37] and GenImage [47] benchmarks. On the GenImage dataset, we train the model using the entire dataset, and we conduct the evaluation on the SDv1.4 subset (images generated by the StableDiffusion model [33]). The evaluated methods are HSJA [5], GeoDA [32], TA [39], ADBA [36], OPT [7], Sign-OPT [8], and our proposed method. The attack models are CNNSpot [37], DenseNet [22], EfficientNet [35], MobileNet [21], ViT [14], Swin Transformer [27], PatchCraft [44], AIDE [40] and Effort [42]. The testing RMSEs are 0.1, 0.05, and 0.01. Our proposed method achieves the optimal attack results. It validates the effectiveness of the integration of adversarial example soups and decision-based attacks based on the frequency-domain signals. The attack effectiveness of our proposed method is more evident on the LSUN dataset [37] than on the GenImage dataset [47]. The potential reason is that the samples of the LSUN dataset are generated by the ProGAN model [23], and the samples of the GenImage dataset are crafted by the StableDiffusion model [33] with more powerful generative abilities. Our method also reveals the adversarial vulnerability of three state-of-the-art AIGC detection models, PatchCraft [44], AIDE [40], and Effort [42].

Figure 2 shows the adversarial example visualization results between our method and other baseline methods, including two frequency-domain-based methods: GeoDA [32] and TA [39]. The noise produced by GeoDA [32] is highly conspicuous, filling the image with random speckles. In contrast, Sign-OPT [8], TA [39], and FBA²D introduce much subtler perturbations. Especially, the experimental results of FBA²D are nearly indistinguishable from the original image. It can be clearly seen that The adversarial examples generated by our proposed method have better concealment.

4.2.2. Frequency Perspectives

Table 3 illustrates the experimental results related to the frequency perspective. The experimental results indicate that, for attacks on real images, selecting 10% of the high-frequency and 10% of the low-frequency components yields the best performance. For attacks on generated images, selecting 20% of the low-frequency components achieves the highest effectiveness.

Dataset	Model	CNNSpot			MobileNet			DenseNet			ViT			EfficientNet		
		RMSE	0.1	0.05	0.01	0.1	0.05	0.01	0.1	0.05	0.01	0.1	0.05	0.01	0.1	0.05
LSUN	OPT	0.768	0.522	0.006	0.836	0.587	0.037	0.666	0.503	0.006	0.748	0.323	0.001	0.703	0.525	0.022
	Sign-OPT	0.170	0.020	0.000	0.296	0.078	0.004	0.176	0.014	0.000	0.259	0.043	0.001	0.226	0.044	0.003
	HSJA	0.809	0.509	0.004	0.541	0.419	0.054	0.497	0.449	0.004	0.958	0.660	0.074	0.527	0.341	0.021
	GeoDA	0.521	0.521	0.346	0.547	0.547	0.485	0.517	0.517	0.389	0.581	0.581	0.473	0.647	0.552	0.349
	TA	0.766	0.673	0.310	0.931	0.889	0.365	0.558	0.551	0.417	0.990	0.985	0.731	0.656	0.558	0.184
	ADBA	0.498	0.494	0.000	0.492	0.477	0.000	0.498	0.489	0.000	0.502	0.497	0.000	0.489	0.475	0.000
	FBA ² D	0.979	0.973	0.909	0.986	0.972	0.796	0.959	0.954	0.874	0.999	0.996	0.777	0.770	0.718	0.491
GenImage	Sign-OPT	0.281	0.087	0.002	0.076	0.015	0.002	0.231	0.052	0.001	0.258	0.115	0.021	0.395	0.113	0.001
	HSJA	0.520	0.410	0.063	0.532	0.324	0.049	0.488	0.337	0.043	0.429	0.275	0.071	0.605	0.490	0.050
	GeoDA	0.658	0.479	0.187	0.803	0.715	0.370	0.555	0.377	0.219	0.527	0.488	0.239	0.668	0.536	0.195
	TA	0.902	0.692	0.221	0.826	0.650	0.216	0.858	0.723	0.266	0.933	0.761	0.367	0.822	0.567	0.113
	ADBA	0.698	0.504	0.000	0.795	0.643	0.000	0.427	0.336	0.000	0.490	0.473	0.000	0.617	0.488	0.000
	FBA ² D	0.908	0.695	0.314	0.962	0.882	0.566	0.999	0.954	0.674	0.905	0.740	0.314	0.923	0.847	0.368

Table 1. Attack Success Rate (ASR) of Different Black-box Attack Methods Across Multiple Models and Datasets part I.

Dataset	Model	Swin Transformer			PatchCraft			AIDE			Effort				
		RMSE	0.1	0.05	0.01	0.1	0.05	0.01	0.1	0.05	0.01	0.1	0.05	0.01	
LSUN	OPT	0.817	0.535	0.002	0.792	0.518	0.003	0.805	0.526	0.002	0.788	0.512	0.004		
	Sign-OPT	0.344	0.028	0.000	0.318	0.025	0.000	0.329	0.026	0.000	0.335	0.027	0.000		
	HSJA	0.676	0.624	0.019	0.692	0.608	0.021	0.684	0.616	0.020	0.688	0.612	0.022		
	GeoDA	0.522	0.522	0.500	0.515	0.515	0.492	0.518	0.518	0.496	0.520	0.520	0.498		
	TA	0.834	0.778	0.299	0.821	0.765	0.285	0.827	0.771	0.292	0.830	0.774	0.295		
	ADBA	0.483	0.473	0.000	0.491	0.481	0.000	0.487	0.477	0.000	0.485	0.475	0.000		
	FBA ² D	0.900	0.890	0.755	0.885	0.875	0.742	0.892	0.882	0.748	0.895	0.885	0.751		
GenImage	Sign-OPT	0.355	0.149	0.002	0.342	0.138	0.001	0.348	0.143	0.002	0.351	0.146	0.002		
	HSJA	0.992	0.839	0.264	0.978	0.825	0.252	0.985	0.832	0.258	0.988	0.835	0.261		
	GeoDA	0.801	0.784	0.343	0.788	0.771	0.331	0.794	0.777	0.337	0.797	0.780	0.340		
	TA	0.547	0.443	0.129	0.534	0.430	0.117	0.540	0.436	0.123	0.543	0.439	0.126		
	ADBA	0.649	0.507	0.000	0.636	0.494	0.000	0.642	0.500	0.000	0.645	0.503	0.000		
	FBA ² D	0.987	0.981	0.891	0.995	0.974	0.868	0.991	0.977	0.879	0.989	0.979	0.885		

Table 2. Attack Success Rate (ASR) of Different Black-box Attack Methods Across Multiple Models and Datasets part II.

4.2.3. Ablation Study

Fig.3 shows the ablation study result of the diverse attack modules. It shows the impact of different initialization methods on attack success rate. For most models, initialization using the sample soup method yields the best results, while initialization using the target attack method yields the worst results. When the RMSE is set to 0.05, the attack configuration of adversarial example soup works is set on most of the target model except in ViT [14]. The potential reason is ViT's architectural divergence from GramNet [26],

the source of the adversarial example soup.

4.3. Discussion

The experimental results show that the frequency-domain dependence of the generated image and the real image is indeed different, which further verifies the basis of our method design. We also find that the decision-based attack method originally used for classification tasks selects the low-frequency (the top 10% low-frequency) as the query subspace, which is an empirically optimal choice. In AIGC detection tasks, there exists a notable distribution discrepancy between the generated image and the real image.

Model	CNNSpot			MobileNet			ViT		
	RMSE	0.1	0.05	0.01	0.1	0.05	0.01	0.1	0.05
10%L	0.53/1.00	0.36/0.99	0.13/0.49	0.86/1.00	0.81/0.97	0.38 /0.35	0.98/1.00	0.97/1.00	0.92/0.53
20%L	0.49/1.00	0.18/1.00	0.06 / 0.69	0.61/0.98	0.47/0.98	0.28/0.82	0.64/1.00	0.58/1.00	0.51 / 0.84
30%L	0.29/1.00	0.07/1.00	0.02/0.61	0.14/0.99	0.09/0.99	0.04 / 0.88	0.47/1.00	0.42/1.00	0.32/0.81
10%H	0.17/0.55	0.03/0.14	0.00/0.03	0.53/0.61	0.23/0.17	0.01/0.02	0.62/0.63	0.20/0.16	0.03/0.02
80%M	0.35/1.00	0.17/1.00	0.07/0.28	0.85/0.99	0.71/0.99	0.35/0.72	0.91/1.00	0.72/1.00	0.27/0.30
10%L+5%H	0.69/1.00	0.52/1.00	0.19 /0.48	0.90/0.98	0.85/0.95	0.32/0.30	0.99 /1.00	0.99 /1.00	0.93 /0.50
10%L+10%H	0.70 /1.00	0.54 /1.00	0.15/0.42	0.95 /1.00	0.90 /0.94	0.28/0.27	0.99 /1.00	0.99 /0.98	0.89/0.44
10%L+15%H	0.68/1.00	0.52/1.00	0.12/0.38	0.91/0.98	0.85/0.91	0.23/0.23	0.98/1.00	0.98/0.97	0.85/0.40

Table 3. ASR of different frequency element combinations.

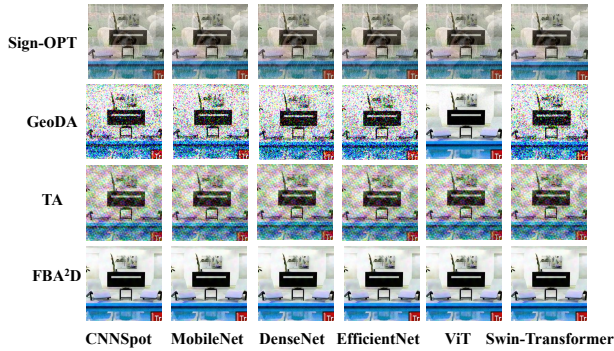


Figure 2. The visualization results of adversarial examples with different method.

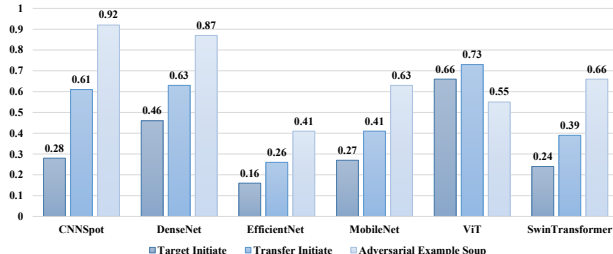


Figure 3. Ablation Study on Different Initialization Methods.

ancy in frequency-domain signal information between real and generated images [2, 16]. When handling real images, the AIGC detection model predominantly focuses on mixed high-low frequency domain information. In contrast, to detect generative images, the model relies mainly on low-frequency components (specifically, the highest 20% lowest frequencies). Although our proposed decision-based black-box attack method has exposed security issues in AIGC applications, current methods still exhibit certain limitations. First, although most adversarial example soup attacks have proven effective, there still exists an “overfitting” phe-

nomenon on ViT and EfficientNet. Second, our frequency-domain signal processing remains empirical and manual, lacking theoretical explanations. Finally, attacks on diffusion models could be more effective.

5. Conclusion

This paper proposes an innovative decision-based attack method for the AIGC detector. Our proposed FBA²D method is guided by the signal decomposition method in the frequency domain. The ensemble of adversarial example soups and initialization with transfer-based attack can improve the efficiency of decision-based attacks. Our evaluation of the Synthetic LSUN dataset and GenImage dataset reveals the security risks faced by the new media industry based on AIGC. Quantitative and qualitative experiments have shown that our proposed method outperforms other attack methods in terms of attack effectiveness and concealment of generated adversarial samples, especially other frequency-domain-based attack methods.

However, our study has certain limitations. First, the transfer-based attacks using the adversarial example soups are not effective against target models whose architectures differ substantially from the source model (e.g., CNN → ViT). Second, although we use CNNSpot to investigate frequency-domain signal characteristics, other models in real-world scenarios exhibit different frequency components compared with CNNSpot.

In future work, we would improve the effectiveness of decision-based attacks against AIGC detectors with diverse architectures. At the same time, exploring paradigms for effective defense is also worthwhile. Investigating the differences between generated and real images in both low- and high-frequency domains and their impact on adversarial robustness warrants further theoretical and empirical study.

FBA²D: Frequency-based Black-box Attack for AI-generated Image Detection

Supplementary Material

In this appendix, we provide more study details relevant to our proposed FBA²D method. The appendix introduces additional experimental settings, and experimental results.

- **Experimental Datasets Additional Information** – Detailed composition of the datasets.
- **Experimental Settings Additional Information** – Description of our choices of experimental settings.
- **Experimental Results Additional Information** — An extended analysis of the experimental results from the main manuscript.

6. Datasets

The Synthetic LSUN dataset contains 720k real images from LSUN and 360k fake images generated by ProGAN [23]. GenImage [46] comprises more than one million pairs of AI-generated fake images and their corresponding real images, spanning all 1,000 classes of ImageNet [9]. These two datasets are crucial benchmarks for understanding the robustness of AIGC.

7. Implementation Details

In our decision-based black-box attack scenarios, we set the momentum decay to 0.95, run for 10 iterations, use a maximum perturbation of $\varepsilon = 8.0/255.0$ and a scaling factor $S_F = 20$. For transfer-based attacks with adversarial example soups, we build the soup by averaging adversarial examples generated by Momentum Integrated Gradients (MIG) [28] on the substitute model GramNet [26] after 6, 7, 8, 9, and 10 iterations. If the adversarial example soup initialization succeeds, we launch the decision-based attack from the clean image using the soup. All hyperparameters for HSJA [5], GeoDA [32], OPT [7], Sign-OPT [8], and ADBA [36] follow their original study settings. The experiments were run on four NVIDIA GeForce RTX 3090 GPUs.

8. Comparison of Frequency Domain Transformation Methods

In this section, we provide experimental results under different frequency-domain transformation methods and analyze the impact of frequency-domain transformation methods on the experimental results. In our experiments, we use two frequency-domain transformation methods. They are Discrete Cosine Transform (DCT), and Discrete Fourier Transform (DFT). We explore different frequency domain transformation methods to assess their impact on the quality of generated adversarial examples. For consistency, we maintain the same experimental procedure. Table 4 illustrates the result that with the 10% L, 20% L, and 10% L + 10% H configurations, the DCT-based method consistently outperforms the DFT-based approach.

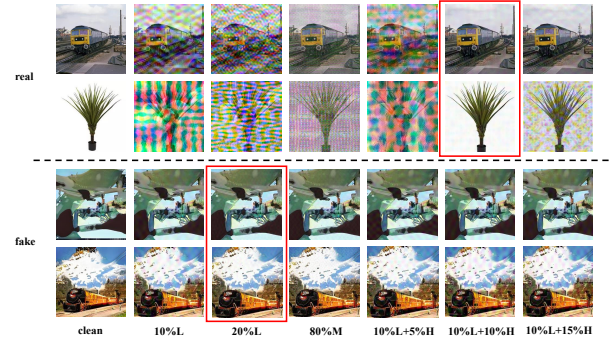


Figure 4. The visualization results of adversarial examples with different frequency element combinations of CNNSpot.

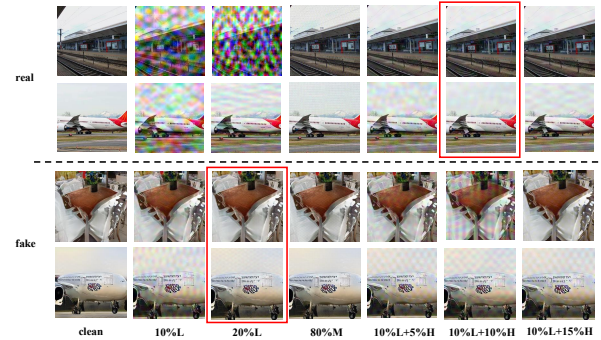


Figure 5. The visualization results of adversarial examples with different frequency element combinations of MobileNet.

trates the result that with the 10% L, 20% L, and 10% L + 10% H configurations, the DCT-based method consistently outperforms the DFT-based approach.

9. Choice of the Number of Adversarial Example Soups' Iterations

This section presents the results for adversarial example soups across different iterations, focusing on two ranges: 6-10 and 8-12. We evaluate our proposed method on the following prominent AIGC detector architectures: CNNSpot [37], DenseNet [22], EfficientNet [35], MobileNet [21], Vision Transformer (ViT) [14], and Swin Transformer [27]. Table 5 shows that the attack initialization effects are comparable. This indicates that, within the range of about 10 steps, increasing the number of iterations yields little improvement in attack performance.

Table 4. Across Multiple Frequency Subspaces Using Different Frequency-domain Transformation Methods on Real (left) and Fake Images (right)

Method	DCT			DFT		
	RMSE	0.1	0.05	0.01	0.1	0.05
10% L	0.533 / 1.000	0.356 / 0.990	0.130 / 0.490	0.348 / 0.984	0.090 / 0.984	0.033 / 0.397
10% L + 10% H	0.697 / 1.000	0.540 / 0.990	0.148 / 0.419	0.517 / 0.995	0.382 / 0.995	0.106 / 0.330
20% L	0.490 / 1.000	0.177 / 1.000	0.057 / 0.687	0.268 / 0.990	0.074 / 0.990	0.024 / 0.351

Table 5. Transfer-based Attack Results after Sample-Soup Augmentation and Clean-Sample Replacement (Average over Iterations 6–10 and 8–12)

Iterations	Target Models & Metrics (ASR / Queries / L2)					
	CNNSpot	DenseNet	EfficientNet	MobileNet	ViT	Swin Transformer
6–10	0.994 / 512 / 2.66	0.966 / 526 / 2.51	0.813 / 701 / 5.20	0.993 / 638 / 4.15	0.999 / 724 / 4.24	0.910 / 574 / 3.44
	0.991 / 511 / 2.58	0.965 / 525 / 2.48	0.789 / 692 / 4.47	0.977 / 631 / 3.84	0.991 / 722 / 4.09	0.908 / 573 / 3.37
	0.919 / 507 / 2.43	0.870 / 508 / 2.23	0.414 / 506 / 2.62	0.630 / 513 / 2.48	0.552 / 504 / 1.49	0.660 / 501 / 2.70
8–12	0.994 / 511 / 2.64	0.966 / 526 / 2.51	0.810 / 701 / 5.20	0.993 / 637 / 4.15	0.998 / 728 / 4.29	0.910 / 574 / 3.44
	0.992 / 510 / 2.59	0.965 / 525 / 2.48	0.789 / 692 / 4.47	0.977 / 631 / 3.84	0.990 / 726 / 4.16	0.908 / 573 / 3.37
	0.919 / 506 / 2.43	0.870 / 508 / 2.23	0.414 / 506 / 2.62	0.630 / 513 / 2.48	0.545 / 502 / 1.49	0.661 / 501 / 2.70

Table 6. PSNR (dB) and SSIM of adversarial examples generated by different black-box attack methods across multiple models and datasets. Higher values indicate better image quality.

Dataset	Method	CNNSpot		MobileNet		DenseNet		ViT		EfficientNet	
		PSNR	SSIM	PSNR	SSIM	PSNR	SSIM	PSNR	SSIM	PSNR	SSIM
ImageNet	Sign-OPT	26.5	0.81	25.8	0.80	27.2	0.83	26.8	0.82	25.3	0.79
	HSJA	29.8	0.87	30.5	0.88	29.3	0.86	28.9	0.85	30.2	0.87
	GeoDA	33.2	0.92	32.7	0.91	33.8	0.93	33.5	0.92	32.4	0.90
	TA	31.1	0.88	30.6	0.87	31.7	0.89	31.3	0.88	30.0	0.86
	ADBA	27.9	0.83	27.3	0.82	28.5	0.84	28.1	0.83	26.8	0.81
	FBA ² D	36.3	0.95	36.8	0.96	35.7	0.94	36.1	0.95	34.9	0.93
GenImage	Sign-OPT	24.2	0.74	23.7	0.73	24.8	0.76	24.5	0.75	23.1	0.72
	HSJA	27.8	0.82	28.6	0.83	27.2	0.81	26.9	0.80	28.3	0.82
	GeoDA	31.4	0.88	30.9	0.87	32.0	0.89	31.7	0.88	30.5	0.86
	TA	29.3	0.84	28.8	0.83	29.9	0.85	29.6	0.84	28.4	0.82
	ADBA	26.1	0.78	25.6	0.77	26.7	0.79	26.4	0.78	25.0	0.76
	FBA ² D	34.1	0.91	34.7	0.92	33.6	0.90	34.0	0.91	32.8	0.89

10. Comprehensive Evaluation of Adversarial Examples’ Perception Quality

In this section, we provide a comprehensive evaluation of the generated adversarial examples from both visual and quantitative perspectives. We first present additional frequency-domain visualizations (Fig. 4 and Fig. 5), revealing that the optimal frequency subspace for real images is 10% L + 10% H elements, whereas for fake images it is 20% L element. These visual results validate our assertion that AIGC images inherently lack high-frequency components, a characteristic effectively leveraged in our attack

methodology, as demonstrated by the red-bordered areas corresponding to the specifically configured frequency subspaces for real and fake images respectively.

To further substantiate the advantage of our method in terms of imperceptibility, we employ the quantitative metrics Peak Signal-to-Noise Ratio (PSNR) and Structural Similarity Index (SSIM) to evaluate imperceptibility. As summarized in Table 6, our method generates adversarial examples with superior perception quality, confirming its enhanced suitability for real-world application scenarios.

References

[1] Wieland Brendel, Jonas Rauber, and Matthias Bethge. Decision-based adversarial attacks: Reliable attacks against black-box machine learning models. In *International Conference on Learning Representations*, 2018. 2

[2] Keshigeyan Chandrasegaran, Ngoc-Trung Tran, and Ngai-Man Cheung. A closer look at fourier spectrum discrepancies for cnn-generated images detection. In *Proceedings of the IEEE/CVF Conference on Computer Vision and Pattern Recognition (CVPR)*, pages 7200–7209, 2021. 2, 3, 6, 8

[3] Jinghui Chen and Quanquan Gu. Rays: A ray searching method for hard-label adversarial attack. In *Proceedings of the 26th ACM SIGKDD International Conference on Knowledge Discovery & Data Mining*, page 1739–1747, New York, NY, USA, 2020. Association for Computing Machinery. 2

[4] Jianbo Chen, Michael I. Jordan, and Martin J. Wainwright. Hopskipjumpattack: A query-efficient decision-based attack. In *2020 IEEE Symposium on Security and Privacy (SP)*, pages 1277–1294, 2020. 2

[5] Jianbo Chen, Michael I. Jordan, and Martin J. Wainwright. Hopskipjumpattack: A query-efficient decision-based attack. In *2020 ieee symposium on security and privacy (sp)*, pages 1277–1294, 2020. 6, 1

[6] Weilun Chen, Zhaoxiang Zhang, Xiaolin Hu, and Baoyuan Wu. Boosting decision-based black-box adversarial attacks with random sign flip. In *European Conference on Computer Vision*, pages 276–293. Springer, 2020. 2

[7] Minhao Cheng, Thong Le, Pin-Yu Chen, Jinfeng Yi, Huan Zhang, and Cho-Jui Hsieh. Query-efficient hard-label black-box attack: An optimization-based approach. *CoRR*, abs/1807.04457, 2018. 2, 6, 1

[8] Minhao Cheng, Simranjit Singh, Patrick H Chen, Pin-Yu Chen, Sijia Liu, and Cho-Jui Hsieh. Sign-opt: A query-efficient hard-label adversarial attack. In *International Conference on Learning Representations*, 2020. 2, 6, 1

[9] Jia Deng, Wei Dong, Richard Socher, Li-Jia Li, Kai Li, and Li Fei-Fei. Imagenet: A large-scale hierarchical image database. In *IEEE Conference on Computer Vision and Pattern Recognition*, pages 248–255, 2009. 1

[10] Yunfeng Diao, Naixin Zhai, Changtao Miao, Zitong Yu, Xingxing Wei, Xun Yang, and Meng Wang. Vulnerabilities in ai-generated image detection: The challenge of adversarial attacks, 2024. 1, 2, 3, 5

[11] Chengdong Dong, Ajay Kumar, and Eryun Liu. Think twice before detecting gan-generated fake images from their spectral domain imprints. In *Proceedings of the IEEE/CVF Conference on Computer Vision and Pattern Recognition (CVPR)*, pages 7865–7874, 2022. 3

[12] Chengdong Dong, Ajay Kumar, and Eryun Liu. Think twice before detecting gan-generated fake images from their spectral domain imprints. In *Proceedings of the IEEE/CVF conference on computer vision and pattern recognition*, pages 7865–7874, 2022. 2

[13] Yinpeng Dong, Fangzhou Liao, Tianyu Pang, Hang Su, Jun Zhu, Xiaolin Hu, and Jianguo Li. Boosting adversarial attacks with momentum. In *Proceedings of the IEEE Conference on Computer Vision and Pattern Recognition (CVPR)*, 2018. 2

[14] Alexey Dosovitskiy, Lucas Beyer, Alexander Kolesnikov, Dirk Weissenborn, Xiaohua Zhai, Thomas Unterthiner, Mostafa Dehghani, Matthias Minderer, Georg Heigold, Sylvain Gelly, et al. An image is worth 16x16 words: Transformers for image recognition at scale. In *International Conference on Learning Representations*, 2021. 5, 6, 7, 1

[15] Tarik Dzanic, Karan Shah, and Freddie Witherden. Fourier spectrum discrepancies in deep network generated images. In *Advances in Neural Information Processing Systems*, pages 3022–3032. Curran Associates, Inc., 2020. 3

[16] Joel Frank, Thorsten Eisenhofer, Lea Schönher, Asja Fischer, Dorothea Kolossa, and Thorsten Holz. Leveraging frequency analysis for deep fake image recognition. In *Proceedings of the 37th International Conference on Machine Learning*, pages 3247–3258. PMLR, 2020. 2, 3, 6, 8

[17] Ian J. Goodfellow, Jean Pouget-Abadie, Mehdi Mirza, Bing Xu, David Warde-Farley, Sherjil Ozair, Aaron Courville, and Yoshua Bengio. Generative adversarial nets. In *Advances in Neural Information Processing Systems*. Curran Associates, Inc., 2014. 1

[18] Ian J. Goodfellow, Jonathon Shlens, and Christian Szegedy. Explaining and harnessing adversarial examples, 2015. 1

[19] Chuan Guo, Jacob Gardner, Yurong You, Andrew Gordon Wilson, and Kilian Weinberger. Simple black-box adversarial attacks. In *Proceedings of the 36th International Conference on Machine Learning*, pages 2484–2493. PMLR, 2019. 2

[20] Jonathan Ho, Ajay Jain, and Pieter Abbeel. Denoising diffusion probabilistic models. In *Advances in Neural Information Processing Systems*, pages 6840–6851. Curran Associates, Inc., 2020. 1

[21] Andrew G Howard, Menglong Zhu, Bo Chen, Dmitry Kalenichenko, Weijun Wang, Tobias Weyand, Marco Andreetto, and Hartwig Adam. Mobilenets: Efficient convolutional neural networks for mobile vision applications. *arXiv preprint arXiv:1704.04861*, 2017. 5, 6, 1

[22] Gao Huang, Zhuang Liu, Laurens Van Der Maaten, and Kilian Q Weinberger. Densely connected convolutional networks. In *Proceedings of the IEEE/CVF Conference on Computer Vision and Pattern Recognition (CVPR)*, pages 4700–4708, 2017. 5, 6, 1

[23] Tero Karras, Timo Aila, Samuli Laine, and Jaakko Lehtinen. Progressive growing of gans for improved quality, stability, and variation. In *International Conference on Learning Representations*, 2018. 6, 1

[24] Seokjun Lee, Seung-Won Jung, and Hyunseok Seo. Spectrum translation for refinement of image generation (stig) based on contrastive learning and spectral filter profile. *Proceedings of the AAAI Conference on Artificial Intelligence*, (4):2929–2937, 2024. 3

[25] Sijia Liu, Pin-Yu Chen, Xiangyi Chen, and Mingyi Hong. signsd via zeroth-order oracle. In *International Conference on Learning Representations*, 2019. 2

[26] Zhengze Liu, Xiaojuan Qi, and Philip Torr. Global texture enhancement for fake face detection in the wild, 2020. 7, 1

[27] Ze Liu, Yutong Lin, Yue Cao, Han Hu, Yixuan Wei, Zheng Zhang, Stephen Lin, and Baining Guo. Swin transformer: Hierarchical vision transformer using shifted windows. In *Proceedings of the IEEE/CVF International Conference on Computer Vision (ICCV)*, pages 10012–10022, 2021. 5, 6, 1

[28] Wenshuo Ma, Yidong Li, Xiaofeng Jia, and Wei Xu. Transferable adversarial attack for both vision transformers and convolutional networks via momentum integrated gradients. In *2023 IEEE/CVF International Conference on Computer Vision (ICCV)*, pages 4607–4616, 2023. 5, 1

[29] Francesco Marra, Diego Gragnaniello, Luisa Verdoliva, and Giovanni Poggi. Do gans leave artificial fingerprints? In *2019 IEEE conference on multimedia information processing and retrieval (MIPR)*, pages 506–511, 2019. 2

[30] Sina Mavali, Jonas Ricker, David Pape, Asja Fischer, and Lea Schönherr. Adversarial robustness of ai-generated image detectors in the real world, 2025. 1, 2

[31] Ali Rahmati, Seyed-Mohsen Moosavi-Dezfooli, Pascal Frossard, and Huaiyu Dai. Geoda: A geometric framework for black-box adversarial attacks. In *Proceedings of the IEEE/CVF Conference on Computer Vision and Pattern Recognition (CVPR)*, pages 8446–8455, 2020. 2

[32] Ali Rahmati, Seyed-Mohsen Moosavi-Dezfooli, Pascal Frossard, and Huaiyu Dai. Geoda: a geometric framework for black-box adversarial attacks. In *Proceedings of the IEEE/CVF conference on computer vision and pattern recognition*, pages 8446–8455, 2020. 6, 1

[33] Robin Rombach, Andreas Blattmann, Dominik Lorenz, Patrick Esser, and Björn Ommer. High-resolution image synthesis with latent diffusion models. In *Proceedings of the IEEE/CVF Conference on Computer Vision and Pattern Recognition*, pages 10684–10695, 2022. 6

[34] Mehrdad Saberi, Vinu Sankar Sadasivan, Keivan Rezaei, Aounon Kumar, Atoosa Chegini, Wenxiao Wang, and Soheil Feizi. Robustness of ai-image detectors: Fundamental limits and practical attacks, 2024. 1, 2, 3

[35] Mingxing Tan and Quoc Le. Efficientnet: Rethinking model scaling for convolutional neural networks. In *International conference on machine learning*, pages 6105–6114, 2019. 5, 6, 1

[36] Feiyang Wang, Xingquan Zuo, Hai Huang, and Gang Chen. Adba: Approximation decision boundary approach for black-box adversarial attacks. In *Proceedings of the AAAI Conference on Artificial Intelligence*, pages 7628–7636, 2025. 6, 1

[37] Sheng-Yu Wang, Oliver Wang, Richard Zhang, Andrew Owens, and Alexei A. Efros. Cnn-generated images are surprisingly easy to spot... for now. In *Proceedings of the IEEE/CVF Conference on Computer Vision and Pattern Recognition (CVPR)*, pages 8695–8704, 2020. 1, 2, 3, 5, 6

[38] Tianyi Wang, Xin Liao, Kam Pui Chow, Xiaodong Lin, and Yinglong Wang. Deepfake detection: A comprehensive survey from the reliability perspective. *ACM Computing Surveys*, 57(3):1–35, 2024. 1, 2

[39] Xiaosen Wang, Zeliang Zhang, Kangheng Tong, Dihong Gong, Kun He, Zhifeng Li, and Wei Liu. Triangle attack: A query-efficient decision-based adversarial attack. In *Computer Vision – ECCV 2022*, pages 156–174, Cham, 2022. Springer Nature Switzerland. 2, 3, 6

[40] Shilin Yan, Ouxiang Li, Jiayin Cai, Yanbin Hao, Xiaolong Jiang, Yao Hu, and Weidi Xie. A sanity check for ai-generated image detection. In *The Thirteenth International Conference on Learning Representations, ICLR 2025, Singapore, April 24-28, 2025*. OpenReview.net, 2025. 5, 6

[41] Zhiyuan Yan, Jiangming Wang, Peng Jin, Ke-Yue Zhang, Chengchun Liu, Shen Chen, Taiping Yao, Shouhong Ding, Baoyuan Wu, and Li Yuan. Orthogonal Subspace Decomposition for Generalizable AI-Generated Image Detection. *arXiv e-prints*, art. arXiv:2411.15633, 2024. 1, 3

[42] Zhiyuan Yan, Jiangming Wang, Peng Jin, Ke-Yue Zhang, Chengchun Liu, Shen Chen, Taiping Yao, Shouhong Ding, Baoyuan Wu, and Li Yuan. Orthogonal subspace decomposition for generalizable ai-generated image detection, 2025. 5, 6

[43] Bo Yang, Hengwei Zhang, Jindong Wang, Yulong Yang, Chenhao Lin, Chao Shen, and Zhengyu Zhao. Adversarial example soups: Improving transferability and stealthiness for free. *IEEE Transactions on Information Forensics and Security*, 20:1882–1894, 2025. 2, 5

[44] Nan Zhong, Yiran Xu, Sheng Li, Zhenxing Qian, and Xinpeng Zhang. Patchcraft: Exploring texture patch for efficient ai-generated image detection, 2024. 1, 5, 6

[45] Ziyin Zhou, Ke Sun, Zhongxi Chen, Huafeng Kuang, Xiaoshuai Sun, and Rongrong Ji. Stealthdiffusion: Towards evading diffusion forensic detection through diffusion model, 2024. 3

[46] Mingjian Zhu, Hanting Chen, Qiangyu YAN, Xudong Huang, Guanyu Lin, Wei Li, Zhijun Tu, Hailin Hu, Jie Hu, and Yunhe Wang. Genimage: A million-scale benchmark for detecting ai-generated image. In *Advances in Neural Information Processing Systems*, pages 77771–77782. Curran Associates, Inc., 2023. 1

[47] Mingjian Zhu, Hanting Chen, Qiangyu Yan, Xudong Huang, Guanyu Lin, Wei Li, Zhijun Tu, Hailin Hu, Jie Hu, and Yunhe Wang. Genimage: A million-scale benchmark for detecting ai-generated image. *Advances in Neural Information Processing Systems*, 36:77771–77782, 2023. 2, 5, 6